DESIGN AND ANALYSIS OF CAPACITIVE MICROMACHINED ULTRASONIC TRANSDUCERS

by

Kendalle Alexia Howard, B.S.

A thesis submitted to the Graduate Council of
Texas State University in partial fulfillment
of the requirements for the degree of
Master of Science
with a Major in Engineering Management
May 2022

Committee Members:

In-Hyouk Song, Chair

Byoung Hee You

Farhad Ameri

FAIR USE AND AUTHOR'S PERMISSION STATEMENT

Fair Use

DEDICATION

I dedicate my thesis work to my family. Special thanks to my father for keeping me grounded, to my mother who cherishes education, to Keirsten for reminding me to push creative boundaries, to Kennadee who is my forever motivator, and to Kaithland for helping me understand my why. Your consistent support and encouragement has not gone unnoticed and I will be forever grateful. I hope this makes you proud.

ACKNOWLEDGEMENTS

I want to express my upmost gratitude to my thesis advisor, Dr. In-Hyouk Song for laying the foundation for my research career. He pushed me to never settle and to continue to strive to reach my goals. His words of encouragement and wisdom has reminded me to remain curious as I progress in my research. He always remind me to “make this research mine” by taking everything I learned from outside sources and break down the concepts until I fully understood them. I appreciate him sharing his extensive knowledge and the financial support throughout my graduate studies. I will forever be grateful and honored to have worked with Dr. Song.

I would also like to express my gratitude to my committee members for their aid during my graduate studies. Their encouraging words and various perspectives have not only been beneficial for me as a student at Texas State University but also as a researcher. Special thanks to Dr. Byoung Hee You and Dr. Farhad Ameri for their attendance at my thesis defense and their feedback.

Lastly, I want to express my gratitude to Lucrecia Ramirez. Her support and friendship during the Summer of 2021 and beyond helped me publish my first research paper, one of my greatest academic accomplishments.

TABLE OF CONTENTS

Page

LIST OF TABLES

Table **Page**

LIST OF FIGURES

Figure **Page**

ABSTRACT

Currently, capacitive micromachined ultrasonic transducers (CMUTs) have emerged as an alternative to the well-established piezoelectric micromachined ultrasonic transducers (PMUTs). The micromachining technology has attracted MEMS researchers to assess the capabilities of CMUT devices to be introduced in various ultrasonic imaging applications. This thesis develops design characterization and simulations for square, hexagon, and circular CMUT cell structures to determine an ideal structure for operating CMUT applications. CMUT cells will be analytically modeled and simulated by Finite Element Modeling (FEM) using COMSOL Multiphysics to highlight the factors influencing the acoustic pressure output maximization. Based on the preliminary results, the hexagon membrane has the highest array packaging density while the more flexible circular membrane has the least amount of stress to operate. This research introduces factors significant for determining the CMUT design for applications with operating frequency ranges of approximately 1.5 MHz.

1. INTRODUCTION

1.1 Background on Capacitive Micromachined Ultrasonic Transducers (CMUTs)

Microelectromechanical systems (MEMS) integrate electrical and mechanical components into miniaturized systems that sense, control and activate mechanical processes to generate large outputs [1]. These systems inexpensively provide ease, low power ratings, quick response times, array fabrication, and increased sensitivity [2]. Micromachined ultrasonic transducers (MUTs) have been introduced in the last few decades to replace piezocomposite ultrasonic transducers using the advantages MEMS-based technology provides [3]. The evolution of this technology provides batch fabrication and an elevated level of integration by integrated circuit (IC) fabrication processes. The scalability improvement expands the use of MUT for wearable or portable devices. This versatility provides an ease in fabricating a wide range of devices that operate at various frequencies, an ideal advantage for MUTs [4]. While operating, the transducers form acoustic waves that imaging systems optimized based on MUT devices' immersion application and functionality of MUTs [5]. There are two miniaturized ultrasonic systems that operate at different actuation principles: a piezoelectric micromachined ultrasonic transducers (PMUTs) and a capacitive micromachined ultrasonic transducers (CMUTs).

PMUTs are comprised of piezoelectric materials enabling the devices to use the piezoelectric effect to detect physical parameters. The physical changes convert into detectable electrical signals in the form of voltage, resonance frequency shift, and charge density [6]. PMUTs excel at performing ultrasonic investigations directly on solids in applications involving nondestructive evaluation. Exciting and detecting ultrasound in fluid mediums with acoustic properties, however, produces a narrow bandwidth and an impedance mismatch resulting in energy loss [7, 8]. PMUT devices require an additional surface matching layer to reduce energy loss from the impedance mismatch further increasing the complexity and manufacturing cost [9]. Although PMUTs have been popularized, the evolution of MUT technology has enabled CMUTs to step in as a competitor of PMUT technology.

CMUT technology has been introduced as alternative technology for imaging and medical applications to overcome the limitation of PMUT devices [10]. CMUT devices improves the impedance matching with surrounding mediums, provides a broader immersion bandwidth, and simplify the fabrication process [11]. Due to how the CMUT is structured in comparison to PMUTs, the ultrasonic waves transmitted are better acoustically matched to surrounding mediums improving sound wave efficiency [4]. Improvement of impedance mismatching can be completed without the an additional surface matching layer [9]. This improvement broadens the immersion bandwidth further impacting axial resolution [7], the increased coupling of sound waves and the sound-bearing mediums [4], and the ability to be integrated with electronic circuits on the same wafer [12]. The miniaturization of CMUT devices allows for the fabrication of on-chip integration possible [4] while reducing noise and providing a wider range of operating temperatures [9]. This considers the ease of manufacturability of the overall production process at lower costs [13].

Although PMUTs have dominated MUT applications [14], the emergence of CMUT technology has created solutions for weaknesses presented by the current ultrasonic transducer. For further advancement of CMUT technology, it is necessary to develop research on the manipulation of CMUT cells and corresponding devices. To develop this research based on background knowledge of CMUTs, two research questions are posed:

- What characteristics of a CMUT will increase the frequency response while decreasing the applied voltage needed to operate efficiently?
- Which geometry (square, hexagon, circular, etc.) produces the highest acoustic pressure output when operating at the same frequency as the natural frequency of the structure?

Considering the questions above, the objective of this research is to design and analyze a CMUT device with the intent of alleviating the limitations presented by other well established CMUTs to produce high level imaging resolution at maximum efficiency. Although the design, analysis, and fabrication of CMUT devices have been implemented for various imaging applications, highlighting the factors influencing the acoustic output of the devices requires additional study. This research intends to analytically model and utilize Finite Element Modeling (FEM) of workable CMUT devices to optimize membrane plate deflection, the durability of the membrane plate, broaden the frequency range workability while operating at full capacity, and increase the acoustic output. This research will develop methods to analyze area utilization of a silicon wafer to increase imaging resolution for transmitting or receiving modes. Organizing CMUT cells within CMUT devices will also improve the directivity of the acoustic output. The acoustic outputs depend on the geometrical factors of the membrane such as area, thickness, and so on. Each shape will be analyzed and simulated.

1.2 Operating Principle of CMUT

A CMUT device is modeled as an array of capacitor cells electrically connected in parallel. As indicated in Fig. 1 (a), each cell consists of a flexible top plate (also referred to as the membrane) with fixed external edges and a rigid bottom plate. An air cavity, separating the two plates, allows the membrane to deflect due to an external force. For the actuation of a CMUT, electrostatic force between the top and bottom electrodes is introduced. The established electrostatic force counteracts the restorative forces of the flexible membrane causing the top electrode to deflect towards the grounded bottom electrode. Figure 1 (b) and (c) are schematics of transmitting mode and receiving mode of CMUT applications, respectively. Indicated in Fig. 1 (b), by additionally superimposing AC voltage along the electrodes, acoustic waves are transmitted into the surrounding medium due to the vibration of the membrane. This continuous vibration operates at the same frequency of the AC voltage. In receiving mode, a DC-bias is required for monitoring a change in capacitance. External acoustic waves cause harmonic modulation of the membrane changing the capacitance of the structure producing a flow of electrical current (Figure 1 (c)) [4].

1.3 CMUT Geometry Comparison

As CMUT technology indicates a promising alternative to the well-established MUT-based technology, researchers focus on generating individual CMUT cells utilizing FEM simulation software, such as COMSOL Multiphysics, and various fabrication techniques [15]. The cells designed are analyzed in a wide range of geometries, materials, and immersion applications to explore the working behavior of the cells based on the parameters set. The types of CMUT cells and their corresponding devices are compared and analyzed for future analysis to identify optimal CMUT design characteristics.

Priya et al. (2015) studied the resonance frequency of a circular polysilicon CMUT structure, but for applications varying from [14] and [16]. The authors sought to design a device ideal for receiving acoustic waves with the intent to utilize the device in medical imaging applications [17]. While analytically modeling and designing the CMUT cells, to increase device operation, a thinner membrane was designed to increase the deformation of the membrane therefore increasing membrane flexibility. The CMUT geometry is validated within COMSOL Multiphysics to establish the frequency at which maximum deformation of the membrane occurs. Additionally, a stress-strain analysis is performed to discover stress and strain levels occurring as the membrane naturally vibrates. Although the CMUT devices [16] and [17] focused on were circular geometries, Sharma et al. (2019) analyzed CMUT structures varying different geometry shapes [18]. The authors performed analytical modeling for the possible geometry shapes comparing the statistical properties of each such as area utilization and membrane plate deflection percentage. Considering the statistical data, square, circular, and hexagonal devices are simulated to identify the eigenfrequencies of each cell however they went into depth about circular cell membranes additionally simulating the electromechanical behavior.

The experimentation and fabrication of an air-coupled hexagonal CMUT was introduced by Aditi et al. (2019) by designing, fabricating, and analyzing individual cells and cell arrays [19]. Utilizing ConvertorWare® tool to design and simulate, numerous factors influencing region of operation were compared and later tested by fabricating a

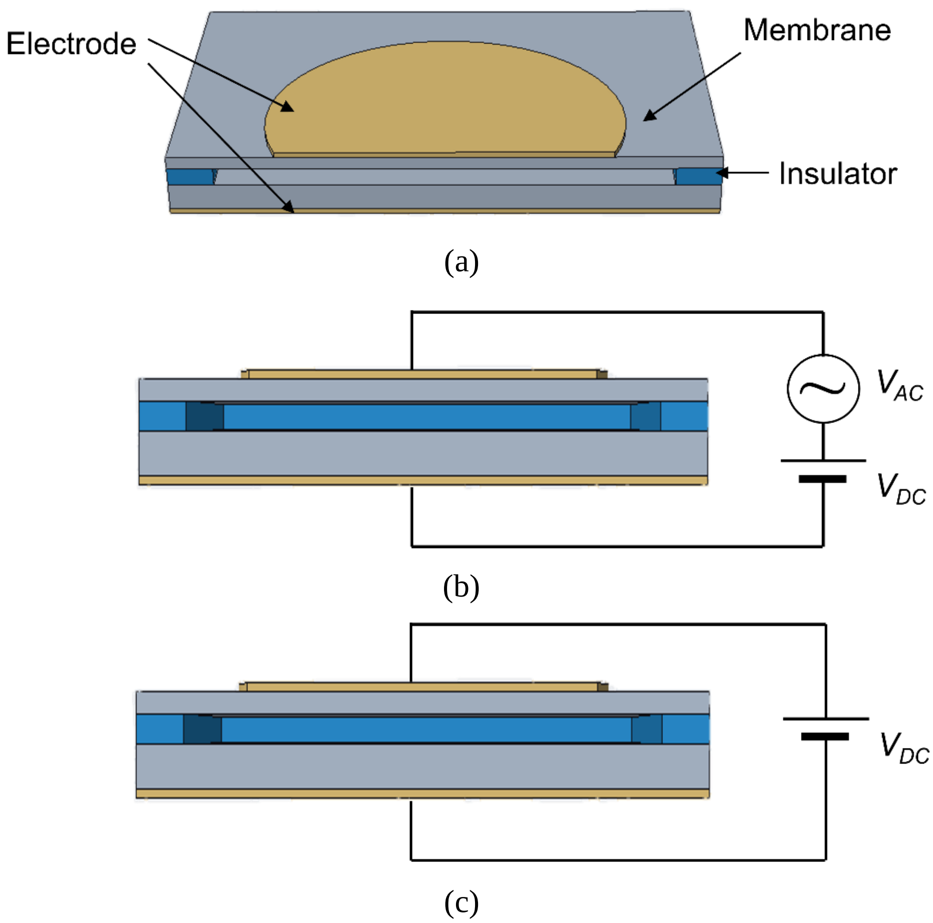

Figure 1. Simplified schematic view of a Capacitive Micromachined Ultrasonic Transducer (CMUT) cell. (a) A CMUT cell composed of a flexible Silicon membrane and Silicon fixed substrate. (b) V_{DC} with a superimposed V_{AC} is applied to the top and bottom Silicon plates during operation causing ultrasonic transmission as the membrane oscillates. (c) External ultrasonic waves cause the Silicon membrane to oscillate while a V_{DC} is applied between the top and bottom electrodes.

device using the anodic bonding technique. Although each hexagonal cell was designed to operate at resonance frequency, approximately 1.44 MHz, an increase resonance frequency occurred as a result of spring hardening effect as membrane thickness and applied DC voltage increased. Based on simulation and experimental data, membrane thickness and the applied DC voltage influences resonance frequency behavior. Additionally, the results indicate the reliability of CMUT devices can be increased during through improving CMUT device design without altering membrane geometry.

Previous research reveals that although the design, analysis, and fabrication of circular CMUT devices has been successfully implemented, other comparable geometry shapes such as square and hexagonal require additional research. To further extend this research, comparison of the three different geometries should be done comparing factors such as mechanical and electromechanical components and each structures' acoustic pressure output. By investigating various geometries shapes and developing methods to improving CMUT devices, the initial gap within previous research will be filled while also highlighting the optimal geometry shape CMUT devices.

2. RESEARCH METHODOLOGY

2.1 Analytical Modeling of CMUT

An investigation of the modeling, designing and corresponding acoustic output are necessary to analyze CMUT device output. The research methodology is an accumulation of quantitative data through analytical modeling and a Finite Element Model (FEM) of three CMUT shapes: square, hexagon, and circular chosen based on review of current research findings [18].

2.1.1 Mechanical Properties

This model focuses on the membrane characteristics of a CMUT cell in addition to the air gap for the calculations while excluding the fixed substrate. Based on the operating principle of a CMUT, the calculated parameters assume a total force, F_T, is applied throughout the surface of the membrane. The total force is an addition of the mechanical force of the flexible membrane and the electrostatic force sourced by the applied voltage ($F_T = F_{me} + F_{el}$). Here, F_{el} is the electrostatic force applied between the two parallel plates induced by an external voltage and F_{me} is the elastic restoring force of the membrane. Operating similarly to a mass-spring-damper system, the membrane is the flexible spring and the attractive forces introduced by the applied voltages drives the mass damping the system. The restorative forces of the membrane, counteracting the attractive forces, are based on the flexural rigidity, *D*, of the membrane. The flexural rigidity influences the membrane deflection when external forces are applied. This value is calculated by [20]:

$$D = \frac{Et^3}{12(1-\nu^2)}, \tag{1}$$

where E and ν, represent Young's modulus and Poisson's ratio of the membrane material respectively and t is thickness of the cell membrane. As the membrane deflects due to an external force, the membrane displaces, x, which can be represented by Hooke's Law:

$$F_{me} = -kx, \tag{2}$$

where k represents the spring stiffness as the membrane undergoes a load. The frequency that allows for maximum deflection of the membrane is the resonance frequency, f_r, or natural frequency of the membrane. This frequency expressed as a function of spring stiffness and the effective mass of the membrane, m_{eff}:

$$f_r = \frac{1}{2\pi}\sqrt{\frac{k}{m_{eff}}}. \tag{3}$$

2.1.2 Electromechanics

When the membrane is at equilibrium with an applied DC bias, the mechanical forces are balanced with the external electrostatic forces as represented below:

$$F_{el} = -F_{me}. \tag{4}$$

As a capacitor-type MEMS device, the electrostatic forces due to DC bias voltage is given by [21]:

$$F_{el} = \frac{\varepsilon A}{2(g-x)^2}{V_{DC}}^2, \tag{5}$$

where ε represents the permittivity of free space, A is the area of the two parallel plates, and g is the air gap distance prior to the applied voltage and x is the displacement of the membrane. When Eq. (4) equates to zero, the summation of Eq. (2) and Eq. (5) develops [15], [22]:

$$V_{DC} = \sqrt{\frac{2kx}{\varepsilon A}}(g - x). \tag{6}$$

Equation (6) considers the relationship between an applied voltage and the membrane displacement. As the CMUT is increasingly biased to a certain voltage value, the top electrode will collapse onto the bottom electrode. This indicates that the attractive electrostatic forces will overtake the mechanical forces of the of the membrane. The voltage value that causes this imbalance between the mechanical forces and electrostatic forces is known as the pull-in voltage, V_{pi}. This imbalance occurs as the membrane displaces 1/3 of the initial air gap ($x = \frac{g}{3}$). Analytical determination of the pull-in voltage for comparative purposes, as shown in Eq. (7), is vital to the design process of a CMUT device to establish sensitivity and the dynamic range of each CMUT cell.

$$V_{pi} = \sqrt{\frac{8kg^3}{27\varepsilon A}} \tag{7}$$

2.1.3 Stress and Strain Relationship

As a CMUT is operating, the dynamic movement of the membrane over an extended period of time influences the stress and strain of the structure. The fixed perimeter of the membrane causes maximum deflection to occur at the center reducing deflection closer to the rigid perimeter. External electrostatic forces, F, introduces tensile stress, σ, perpendicularly to the structure.

$$\sigma = \frac{F}{A} \tag{8}$$

The change in electrostatic forces applied to the structure will influence the tensile stress based on the area of the membrane, A, and external force applied. As tensile stresses are introduced, the membrane deforms elongating the length, L, of the membrane in proportion to the applied electrostatic force known as the tensile strain, ε. The higher the displacement distance of the membrane, the higher the strain acted upon the structure.

$$\varepsilon = \frac{\Delta L}{L} \tag{9}$$

The relationship between tensile stress and tensile strain of the Silicon membrane is Young's modulus to determine the stiffness of the structure. The significance of the stress and strain relationship of a Silicon CMUT cell is to indicate the behavior of the membrane as external forces are applied. This relationship identifies the yield strength of the structure meaning the point at which the external forces overtake the restorative forces of the structure causing permanent damage to the structure. Based on a single-crystal Silicon membrane, the yield tensile strength is approximately 170 MPa. Any stress levels produced above 170 MPa will cause permanent damage to the membrane structure [23].

2.1.4 Acoustics

The collection of molecules in fluid mediums, specifically air, are in random constant motion without external forces applied. Once applied, there is an increase in pressure as the medium molecules interact with the mechanical disturbance. In this context, the source of the disturbance is replaced with a CMUT. This constant motion develops zones of compression and rarefaction propagating ultrasonic waves due to the motion of molecules moving in parallel to the direction of the wave propagation. The ultrasonic waves transmit into surrounding mediums at frequency levels greater than 20 kHz, the upper limit audible ranges for humans [24]. The fluctuations from the designated static pressure of the medium are due to the infiltrating sound waves. Each wave cycle operates at a designated frequency developed by the wave equation expressed as:

$$c = f\lambda, \tag{10}$$

where c, f, and λ are the speed of sound, frequency, and wavelength, respectively. As the sound waves propagate, the acceleration of the waves is the largest amplitude reached in one acoustic cycle. As the sound waves propagate, the diminishing intensity is related to the surrounding medium, temperature, distance of propagation from source point, and the wave cycle frequency. For air mediums, attenuation loss as a function of frequency have a proportionate relationship resulting in an increase in attenuation loss as frequency increases [25].

It is widespread practice to reference acoustic ranges in terms of sound level considering sound pressure values can have large value ranges [26]. The value of Sound Pressure Level (SPL) represents the acoustic wave strength produced by the CMUT membrane as given by:

$$SPL = 20\, log(\frac{p}{p_{ref}}). \tag{11}$$

Here, p is the sound pressure measured in rms and p_{ref} is the reference sound pressure. Considering the known hearing threshold for humans is approximately 1 kHz, the reference sound pressure for SPL is 20 µPa. Developed as a ratio, when sound pressure equals the reference sound pressure this corresponds to a 0 dB SPL [24]. To compare the acoustic outputs of each CMUT structure designed, a frequency sweep will be conducted steadily increasing the frequency in the ultrasonic ranges. Based on the SPL transmitted, the acoustic pressure, p, produced by a CMUT cell can be extracted by this equation:

$$p = 10^{\frac{SPL}{20}} \times 20\ \mu Pa. \tag{12}$$

2.2 Design and FEM Simulation

Based on previous research mentioned in Section 1.3, three CMUT cell geometries have been popularized as CMUT membrane designs: square, hexagonal, and circular. This paper introduces analytical and simulated comparisons among each geometry considering various parameters such as cell size, resonance frequency, electrostatic force, and acoustical outputs. Finite Element Modeling (FEM) of each CMUT cell is constructed using COMSOL Multiphysics software to solve for complex physical interactions. Structural mechanics and electrostatic domains coupled are utilized to quantify and visualize the mechanical and electromechanical behaviors of each CMUT cell. Acoustic-Structure Interaction physics is also utilized simulating the interaction between the vibrating CMUT membrane and the surrounding air medium. This interprets the change in medium pressure due to the acoustic output from the CMUT membrane.

The designed CMUT device will later be fabricated using IC processes such as UV-lithography, etching, wafer bonding, and deposition on silicon wafer [26, 27]. So, each 3D cell is simplified to be comprised of a Si membrane fixed along the perimeter and an enclosed air gap when testing mechanical and electromechanical properties. An additional air dome with a perfectly matched layer (PML) incapsulates the membrane and air gap to assess the acoustic pressure output from each CMUT cell. The PML is an absorbing boundary utilized to emulate the radiation of spherical waves without producing reflection [15, 28].

Beyond highlighting the most optimal geometrical shape for CMUT devices, our goal is to also design CMUT cells that will operate at a fixed resonance frequency of 1.5 MHz. Based on the analytical model, membrane material properties, and membrane radius and thickness are a function of resonance frequency. Understanding this, the first step was to determine the optimal dimensions for a CMUT cell that will have a resonance frequency of 1.5 MHz. In COMSOL, resonance frequency as a function of side length and radius was simulated referred to as a modal analysis.

The modal analysis performed results in a fixed number of eigenfrequencies or mode shapes. The mode shape that is selected represents the frequency at which the membrane has maximum deflection. Table 1 describes the material properties compiled by the material library provided by COMSOL for a single crystal Silicon membrane. Table 2 represents the acoustic specifications inputted in COMSOL in addition to Table 1 parameters.

Table 1. Mechanical Specifications for Simulation

Material	Silicon
Thickness of Si membrane, t	1.5 µm
Initial Air Gap, *g*	0.5 µm
Density of Si, ρ	2330 kg/m^3
Young's Modulus of Si, *E*	170 GPa
Poisson's ratio of Si, ν	0.28
Relative permittivity of Si	11.7

Table 2. Acoustic Specifications for Simulation

Parameters	Values
Air Dome Radius	1000 μm
Speed of Sound	343 m/s
Temperature	293.15 K
Absolute Pressure	1 atm
Source acceleration	1000 m/s^2
Perfectly Matching Layer (PML)	100 μm

2.2.1 Square

For simulating square shape, the side length, a, is increased from 100 μm to 200 μm with a fixed membrane thickness of 1.5 μm. This resulted in a resonance frequency range of 2.2 MHz to 0.5 MHz. The geometrical design and the plot of resonance frequency as a function of side length are shown in Fig. 2. To obtain a resonance frequency of approximately 1.5 MHz, a side length of 121.25 μm is simulated.

2.2.2 Hexagon

The hexagonal membrane is designed for the radius of the inscribed circle of the hexagon to equate to its side length, a, by inputting the equation in COMSOL below:

$$r = \frac{\sqrt{3}a}{2}, \tag{11}$$

where 'r' refers to the radius of the inscribed circle of the hexagon membrane in μm and 'a' is the side length in μm. The side length is increased from 50 μm to 100 μm with a fixed membrane thickness of 1.5 μm resulting in resonance frequencies of 3.2 MHz to 0.8 MHz. The geometrical design and the plot of resonance frequency as a function of side length are shown in Fig. 3. Developing a side length of 72.25 µm will create a hexagonal membrane that operates at a resonance frequency of approximately 1.5 MHz.

2.2.3 Circular

For the simulation of a circular membrane, the membrane is designed to steadily increase the membrane radius, *r,* from 50 µm to 100 µm with a fixed membrane of 1.5 µm resulting in a resonance frequency range of 2.6 MHz to 0.6 MHz. The geometrical design and the plot of resonance frequency as a function of radius are shown in Fig. 4. To obtain a resonance frequency of 1.5 MHz, a radius of 64.65 µm and a diameter of 129.3 µm is utilized for the simulation.

Once each of the CMUT cell dimensions are obtained to correspond with 1.5 MHz, the first three eigenfrequencies are simulated as shown in Table 3. The first eigenfrequency indicates the cell has a maximum deflection point at the center of the membrane, ideal for CMUT devices. The second and third eigenmodes occur at higher frequencies with a 90-degree difference between the two eigenmodes for each CMUT shape. The center of the membranes have little to no deflection. The first eigenfrequency is selected and therefore the membrane sizes chosen for further analysis for square, hexagon, and circle are 121.25 µm, 144.5 µm and 129.3 µm, respectively.

2.3 Resonance Frequency Mesh Convergence Test

While analytical modeling provides quick analysis of the characteristics of a CMUT, it only considers the linear properties of the device. Simulation using FEM counteracts the analytical modeling limitations while providing better visualization of the behavior of a CMUT cell as the parameters and various functions are adjusted. The accuracy of the

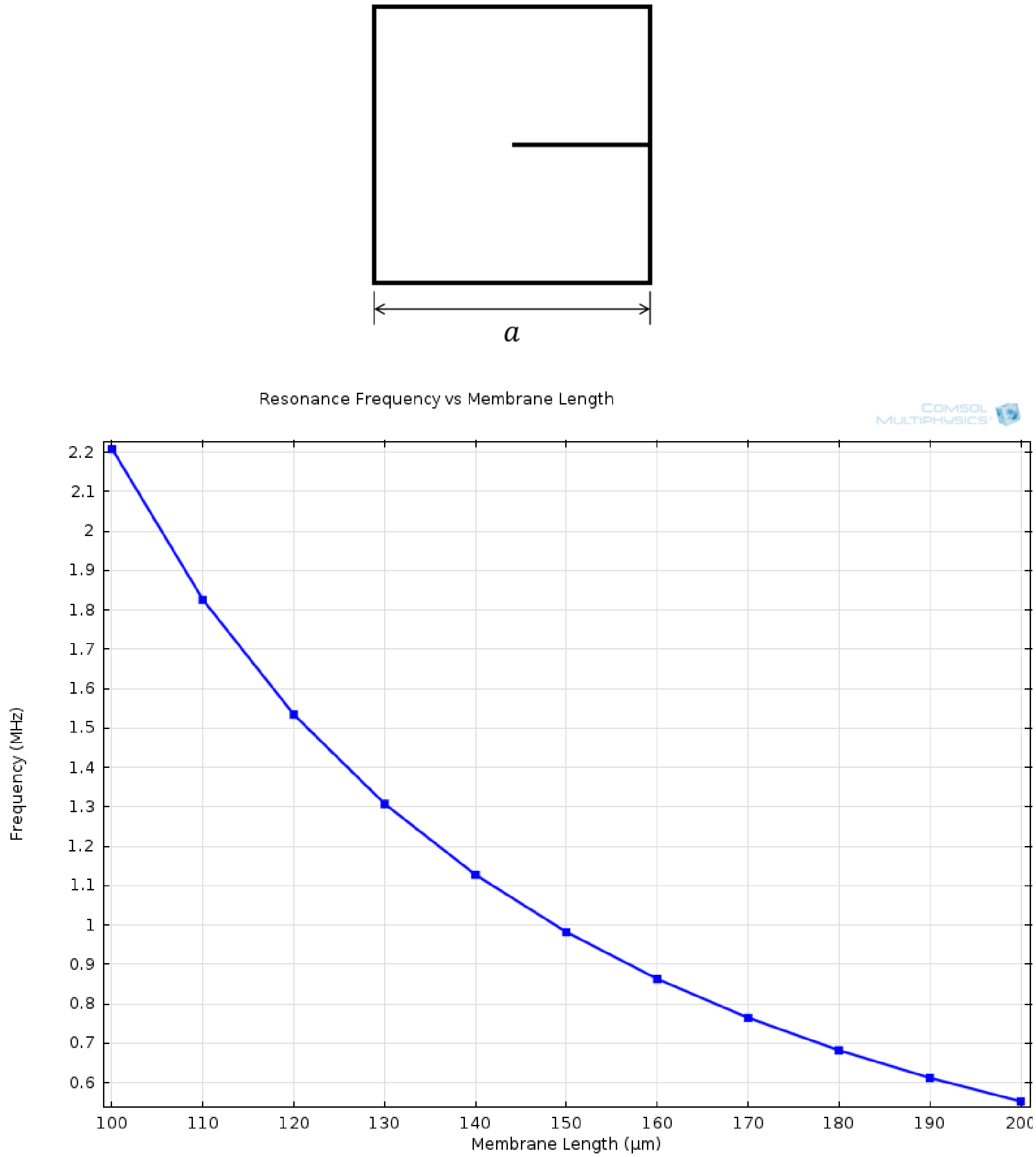

Figure 2. Design of square CMUT cell and resonance frequency as a function of side length, a, of square CMUT cell.

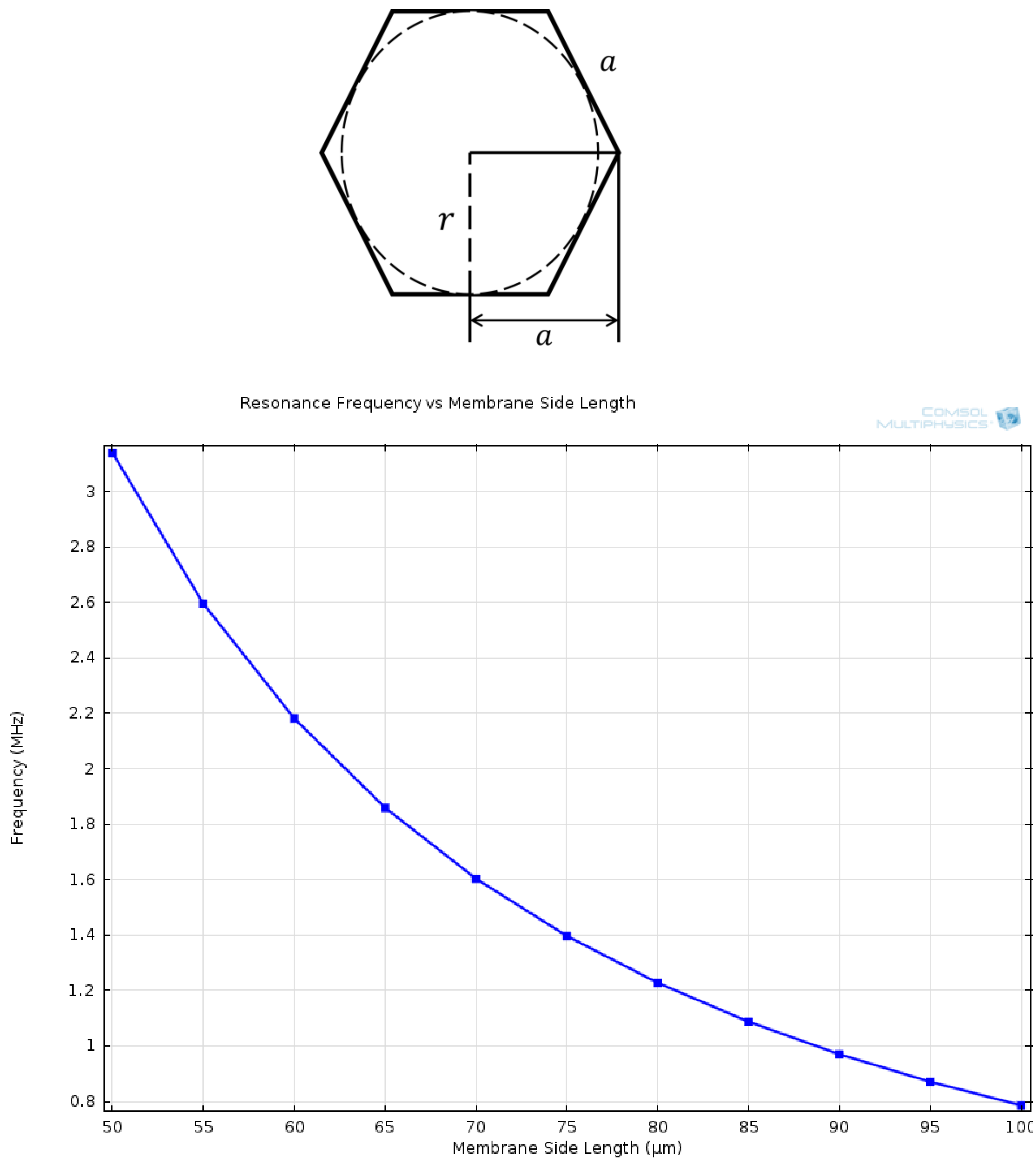

Figure 3. Design of hexagon CMUT cell and resonance frequency as a function of side length, a, of hexagon CMUT cell.

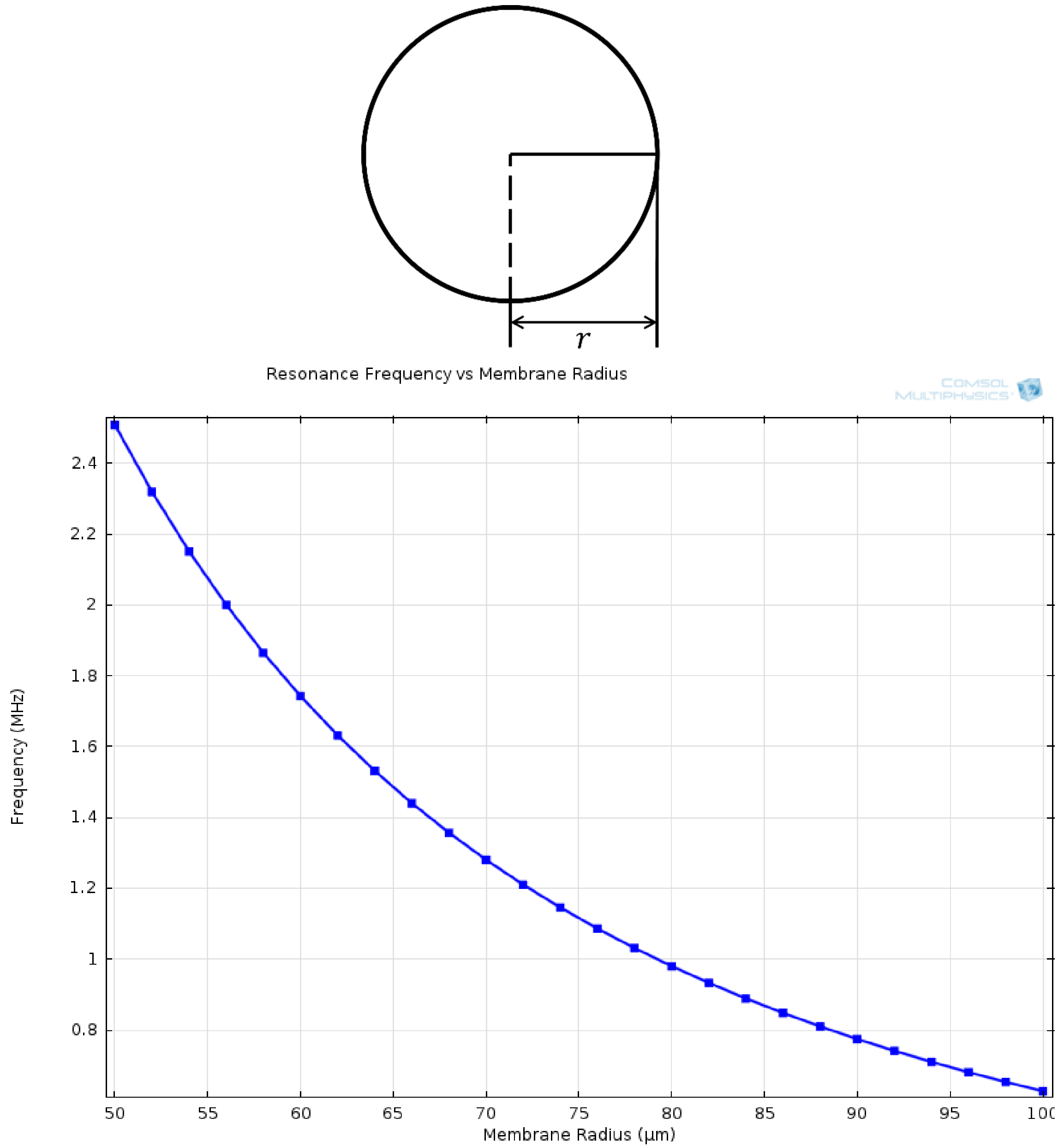

Figure 4. Design of circular CMUT cell and resonance frequency as a function of membrane radius, r, of circular CMUT cell.

Table 3. Geometrical Specifications for Different Membrane Shapes

Specifications	Square	Hexagon	Circular
Shape Dimensions	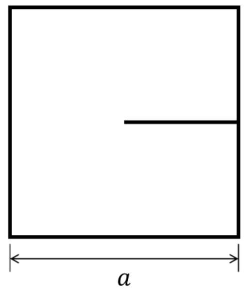	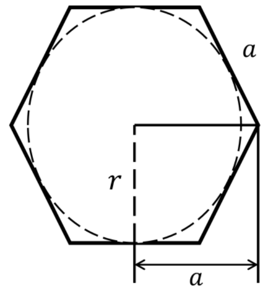	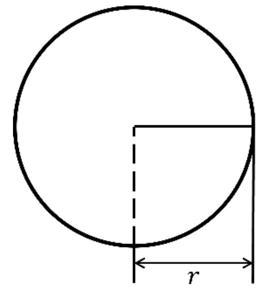
Cell Size	a = 121.25 μm	2a = 144.5 μm	2r = 129.3 μm
1st Mode Eigenfrequency	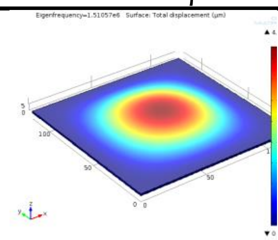	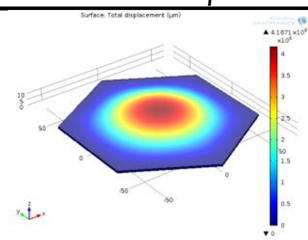	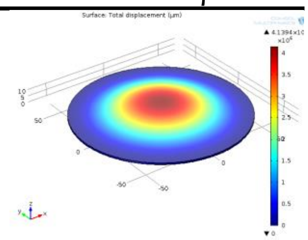
	1.51 MHz	1.52 MHz	1.49 MHz
2nd Mode	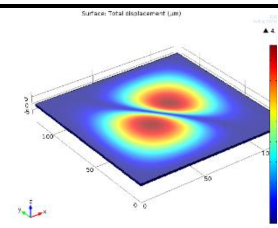	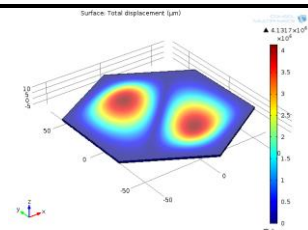	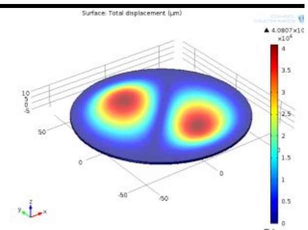
	3.079 MHz	3.142 MHz	3.09 MHz
3rd Mode	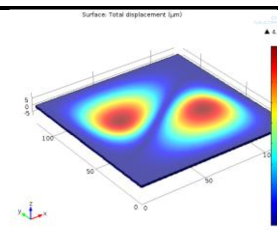	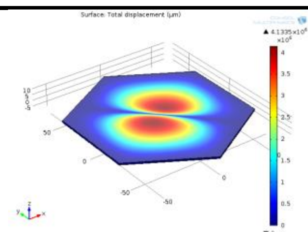	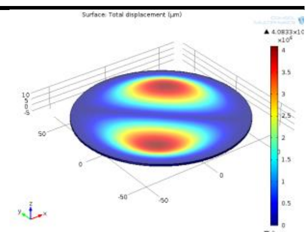
	3.079 MHz	3.142 MHz	3.09 MHz

solutions produced rely on mesh size or the number of elements that solve various differential equation to produce a solution. Proportionately, as mesh size increases, closer to model an infinite element size, the equations solved move closer to the exact solution. Due to this research relying on the COMSOL solutions to analyze CMUT devices, a mesh convergence test (MCT) is performed.

Due to the modal analysis influencing the design structure of the three CMUT geometries, a MCT is performed with the goal of defining the cell dimensions closest to the frequency of 1.5 MHz. COMSOL has built-in meshing parameters ranging from finer mesh element size to coarser mesh element size. The finer the mesh, the more elements are distributed across the cell. The relationship between the number of elements and the resonance frequency is simulated and the results are compared in Fig. 5. Based on the results, the mesh size that results in a solution closest to 1.5 MHz will be the mesh size selected.

As shown, as the number of mesh elements increase, the resonance frequency decreases for all three CMUT cell geometries. The percent difference between the finer mesh (maximum number of elements) and coarser mesh (minimum number of elements) for square, hexagon, and circular are 0.7%, 0.3%, and 0.6%, respectively. Considering the increase in mesh elements results influences resonance frequency at less than one percent, the mesh size utilized for future simulation has less than 100,000 elements but greater than 30,000 elements.

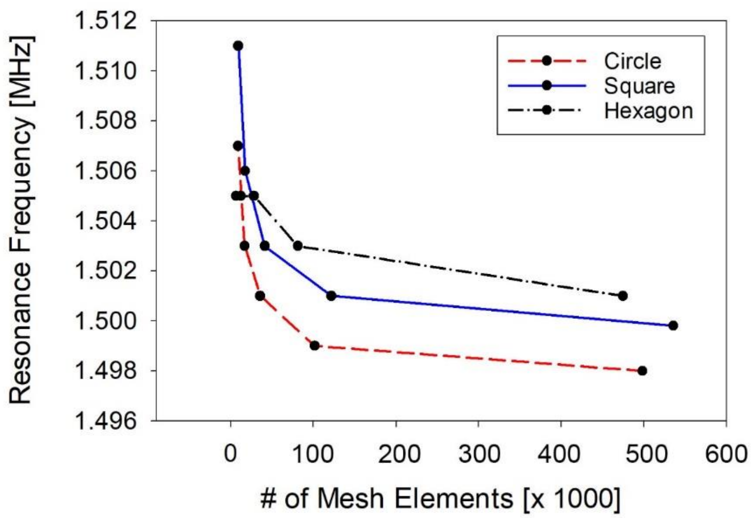

Figure 5. The change in resonance frequency versus change in number of mesh elements for square, hexagon, and circular membrane geometries.

3. RESULTS AND DISCUSSION

3.1 Array Density Comparison

When integrating CMUT devices, the array of cells will be arranged on a 1 cm × 1 cm silicon wafer. Based on the FEM results, each CMUT array is constructed in Autodesk AutoCAD as partially shown in Fig. 6. The dimensions for each cell are mentioned in Table 3 to operate at 1.5 MHz of resonance frequency. For maximum operating efficiency, the number of cells positioned is based on individual cell spacing and geometry specifications. Each cell is evenly spaced 50 µm until equal distribution of cells is beyond the 1 cm × 1 cm area. Table 4 shows the array comparison for each CMUT shape. The resulting constructed arrays indicate CMUT devices fabricated with hexagonal membranes maximize wafer area with 4,037 cells occupying 55% of the wafer, followed by square at 3,364 cells occupying 49 %, and circular with 3,608 cells occupying 47%. The hexagon membrane most efficient in terms of density of the 1 cm x 1 cm silicon wafer.

Table 4. CMUT Array Comparison for Three Membrane Geometries

Geometry	Area	# of cells/cm^2	Occupied Area
Square	14.70 nm^2	3364	49%
Hexagon	13.56 nm^2	4037	55%
Circular	13.13 nm^2	3608	47%

3.2 Spring Stiffness

The objective of determining the spring stiffness of each shape is to highlight the cell membrane with the highest flexibility, meaning the lowest stiffness value. A lower

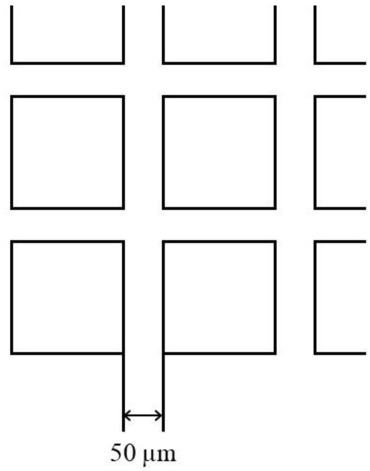

(a)

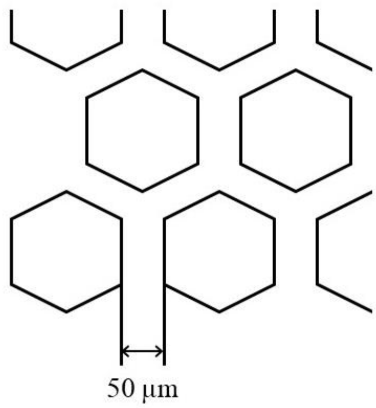

(b)

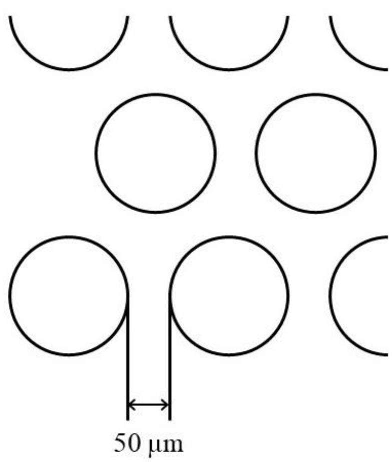

(c)

Figure 6. Three array configurations of (a) square, (b) hexagon, and (c) circular CMUT cells spaced 50 μm apart.

stiffness indicates that the corresponding membrane will displace more under the same applied force in comparison to the other CMUT shapes. To extract the spring stiffness of each cell membrane, a fixed constant pressure of 500 nN is distributed evenly across the cell membrane perpendicular to the static membrane. This constant external force in the negative z-coordinate direction results in various displacements for each geometry membrane.

The spring stiffness of each membrane is derived using Eq. (2), Hooke's Law. Based on the applied conditions, the square geometry deflects the least displacing 0.18 nm resulting in a higher spring stiffness of 2787 N/m. The maximum deflection at 0.20 nm is shown by the circular membrane resulting in a spring stiffness of 2495 N/m. Additionally, the hexagon membrane generated a spring stiffness of 2597 N/m when displaced at 0.19 nm. The rigidity of the square membrane is greater in comparison to circular and hexagon structures indicating less external force is required to reach maximum displacement for circular cell membranes.

3.3 Electromechanics Comparison

Obtaining the pull-in voltage highlights the dynamic limitations of the CMUT membranes while in operation. The solid mechanics and electrostatics physics are added to each geometry with the proper parameters applied. Each CMUT cell geometry simulated has an initial air gap of 0.5 μm when 0 V is applied across the structure. To simulate pull-in voltage for each individual cell, a global equation is applied to find a solution for the inverse equation below.

$$intop1(z) - zset = 0 \tag{13}$$

As stated regarding the operating principle of a CMUT, as an applied DC voltage increases, the membrane will displace towards the substrate. Due to maximum deflection occurring at the center of the membrane, an integration point, $intop1$, is applied to mark the membrane center. By applying this equation, COMSOL solves for the DC voltage needed to cause the integration point to displace at a set z-coordinate, $zset$.

The results of this computation, as indicated in Fig. 7, is the z-coordinate displacement versus pull-in voltage curve that corresponds with the minimum voltage. The highest pull-in voltage value is the hexagonal membrane at 34.46 V followed by square at 34.38 V and lastly, circular at 34.39 V. Although pull-in voltage is an influential factor in determining the optimal CMUT design the pull-in voltage results indicate a less than one percent difference between the cell geometries.

To derive the electrostatic forces utilizing Hooke's Law equation and the derived spring stiffness values in Section 3.2, a consistent V_{DC} voltage among all three geometries. It is also necessary to consider that the voltages must be lower than the pull-in voltage values because the membrane will collapse at voltages above the simulated values. Meeting this criteria, 30 V is applied while allowing for an electrostatic force comparison. Under the same constant voltage, all three membranes displaced at approximately 0.12 μm. Given the displacement, the electrostatic force generated is calculated. The results for the electromechanical behaviors of all three cell geometries are shown in Table 5. The square geometry generates the highest electrostatic force of 325 μN to displace at 0.12 μm. This is due to the square membrane having a more rigid membrane in comparison to the other two cell geometries. This indicates that the square membrane requires a greater amount of force to displace. The circular and hexagon membranes are more pliable in comparison also indicated by the spring stiffness values. The circular membrane, however, generated 290 µN of force validating that the circular membrane is more pliable than hexagon membrane (300 µN) and square membrane.

Table 5. Electromechanics for Three Membrane Geometries

Geometry	Pull-in Voltage	Applied DC Voltage	Displacement at 30 V	Electrostatic Force at 30 V
Square	34.38V	30 V	0.12 µm	325 µN
Hexagon	34.46 V	30 V	0.12 µm	300 µN
Circular	34.39 V	30 V	0.12 µm	290 µN

3.3.1 Electromechanics Mesh Convergence Test

In Section 2.3, a MCT is performed to highlight the optimal element size for CMUT cells with a goal resonant frequency of 1.5 MHz. In this section, an additional MCT is performed with the same parameters however this section highlights the relationship between the number of mesh elements and the displacement of each geometry membrane with an applied V_{DC} of 30 V. As shown in Fig. 8, the displacement steadily increases as number of mesh elements increases for all three CMUT cell geometries. The percent difference between the finer mesh (maximum number of elements) and coarser mesh (minimum number of elements) for square, hexagon, and circular are 2.1%, 3.1%, and 1.9%, respectively. Based on the percentages, the meshing selected for electromechanical simulations is finer than the meshing for resonance frequency simulations. The mesh size utilized for future simulation has more than 100,000 elements for accurate results.

3.4 Stress and Strain Distribution

As a microscale structure that vibrates within ultrasonic ranges, a stress and strain analysis is simulated strictly on the moving components of the CMUT cell. To obtain consistent results, 30 V is once again applied to each membrane geometry to visualize and quantify the effects of adding electrostatic forces to the membrane without the possibility of permanently deforming the membrane. The perimeter of each membrane is fixed with an assumption that the maximum deflection point is at the center of each membrane and decreases when the deflection point travels closer to the perimeter. For comparison, each membrane is cut in half to plot the stress and strain variation while under the electrostatic forces produced by 30 V.

Figure 9 and 10 visually indicate the stress and strain distribution of each membrane shape in addition to quantifying the maximum stress levels, respectively. The dark red color indicates the highest values in pascals (Pa) while dark blue represents the lowest. The simulation results conclude that as each membrane deflected in the negative z-coordinate direction (towards the substrate), there is a higher concentration of stress in the center of the sides of the square membrane at approximately 36.55 MPa followed by hexagon at approximately 34.42 MPa. The lowest levels of stress occurred in the corners. In contrast, the circular membrane has an equal distribution of stress around the perimeter at approximately 26.07 MPa. The electrostatic forces applied to the square and hexagon have a greater impact on the dark red sections of the membrane. Considering the applied voltage is below pull-in voltage, the strain is higher at around the perimeter of each membrane as the membrane elongates in the negative z-coordinate direction.

3.5 Acoustic Pressure Output

To analyze the phenomenon of sound pressure generated from CMUT devices, the acoustic-structure interaction physics is utilized coupling the mechanical parameters with the addition of an air dome and a perfectly matched layer (PML). It is significant to note that the CMUT cells simulated have a source acceleration boundary applied to the top of the membrane to identify the source of the acoustic pressure. The source acceleration value applied follows the principles of the acceleration of a vibratory body [29]. The membrane is vibrated at resonance frequency (1.5 MHz). It is assumed that CMUT cell devices operate well at resonance frequency producing the maximum amount of membrane deflection resulting in the greatest acoustical output possible [13, 30]. Additionally, it is assumed that as the distance through the air medium increases from the membrane, the acoustic pressure decreases.

Figure 11 (a) represents the circular geometry designed based on the geometrical specifications in Table 2. Figure 11 (b) represents the meshing applied to the geometry based on COMSOL. Triangular meshing is applied to the entire geometry apart from the PML. A swept mesh with proper element distribution is applied to the remaining geometry [28]. Square and hexagon cell geometries were designed and meshed with the same parameters. The total acoustic pressure within the air dome is simulated and plotted in 2D to visualize the sound wave propagation at 1.5 MHz generated by the three cell geometries. As shown in Fig. 12., the maximum acoustic pressure generated was the circular membrane at 47.95 Pa, followed by hexagon at 47.50 Pa and square at 46.00 Pa. As established previously in, the circular membrane is the more pliable membrane in

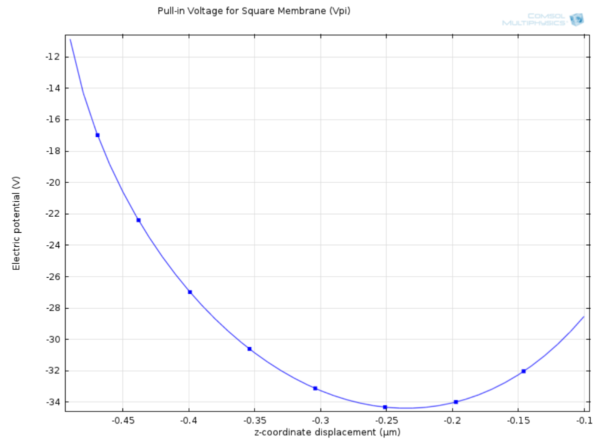

(a)

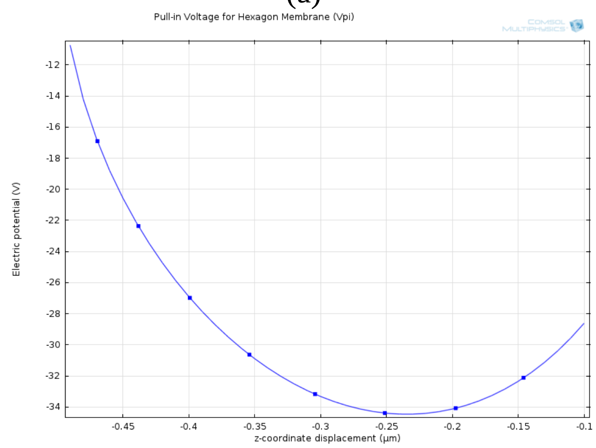

(b)

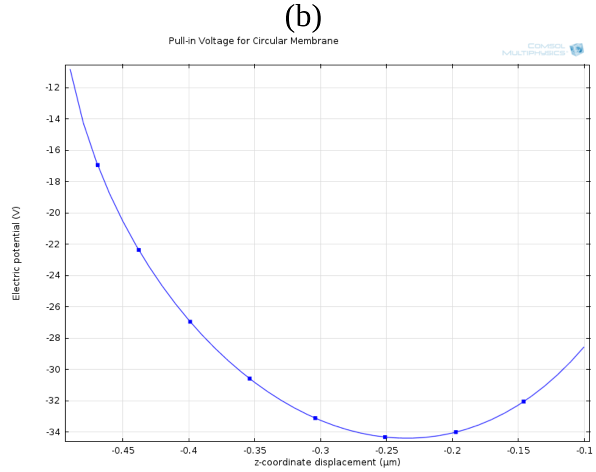

(c)

Figure 7. Simulated pull-in voltage required to compute a set displacement for three CMUT cell geometries. The minimum voltage for (a) square at 34.38 V, (b) hexagon at 34.36 V, and (c) circular at 34.39 V are the pull-in voltages.

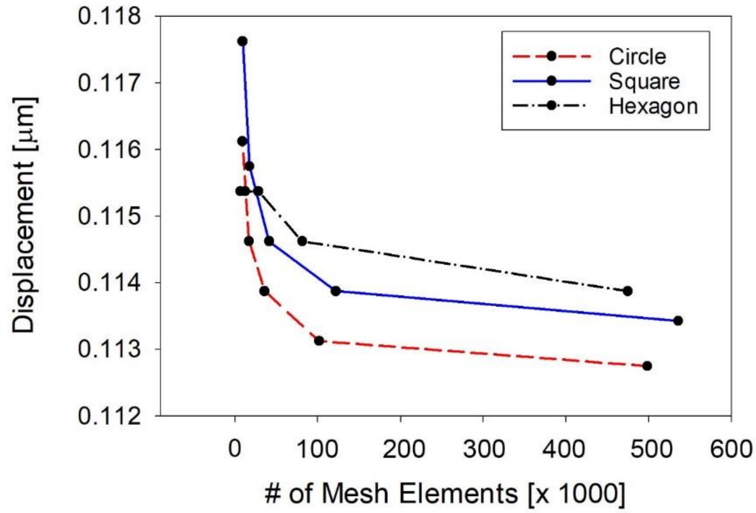

Figure 8. The change in displacement at 30 V versus change in number of mesh elements for square, hexagon and circle membrane geometries.

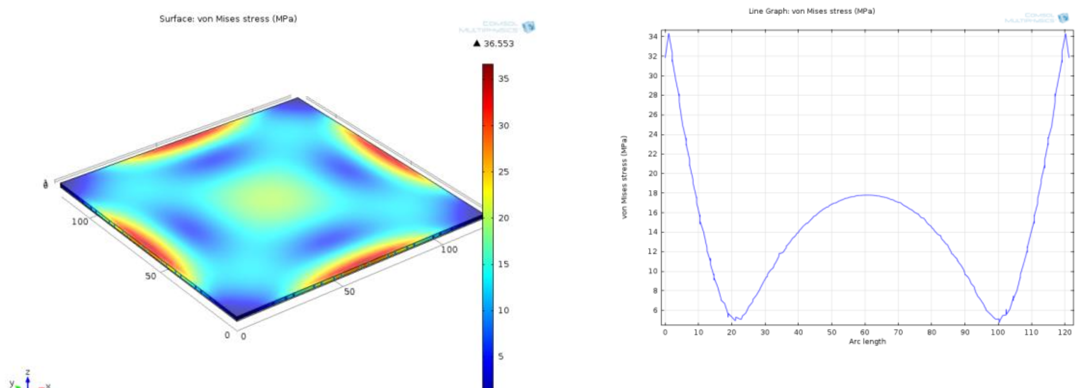

36.55 MPa (Edge)
17.8 MPa (Center)

(a)

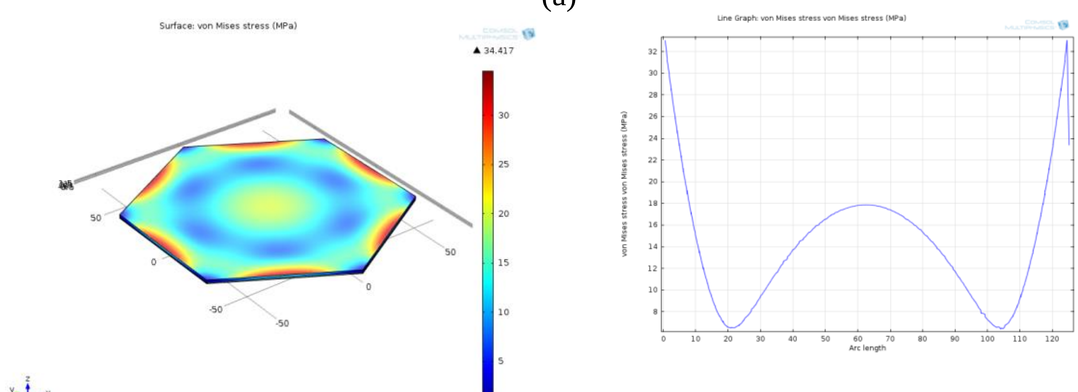

34.42 MPa (Edge)
17.85 MPa (Center)

(b)

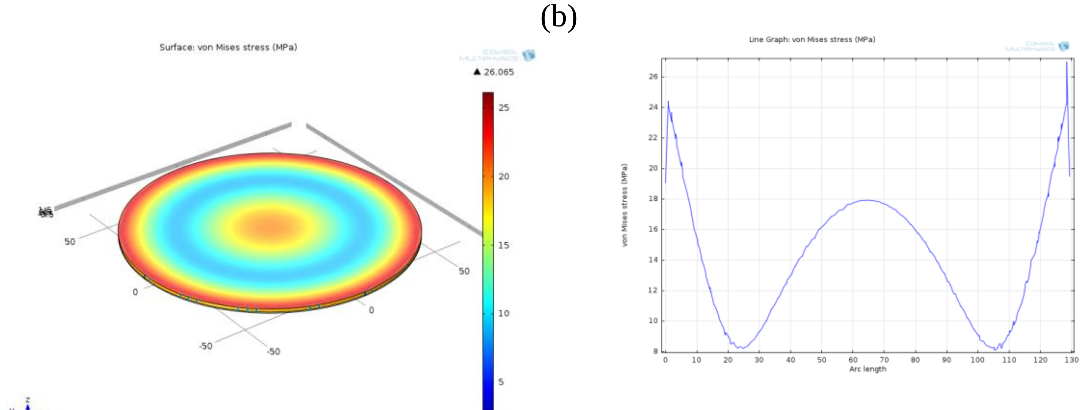

26.07 MPa (Edge)
17.91 MPa (Center)

(c)

Figure 9. Simulated stress analysis of (a) square, (b) hexagon, and (c) circular CMUT membranes.

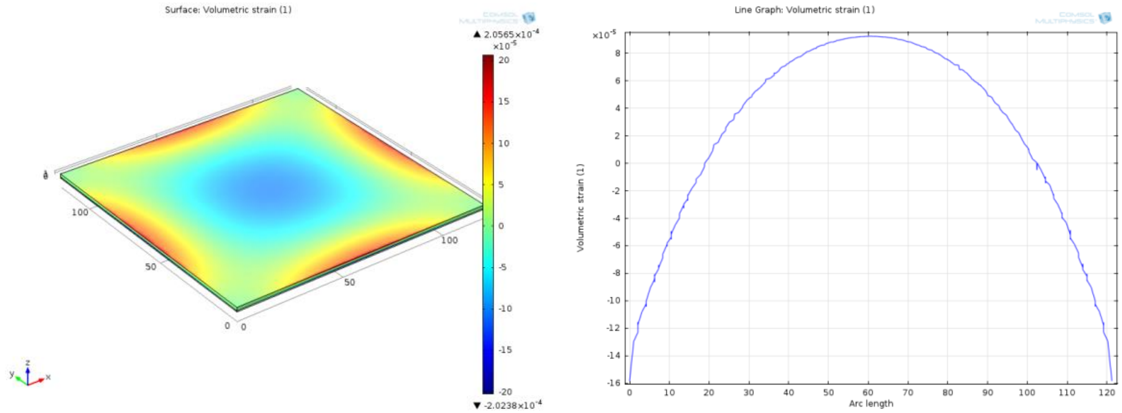

(a)

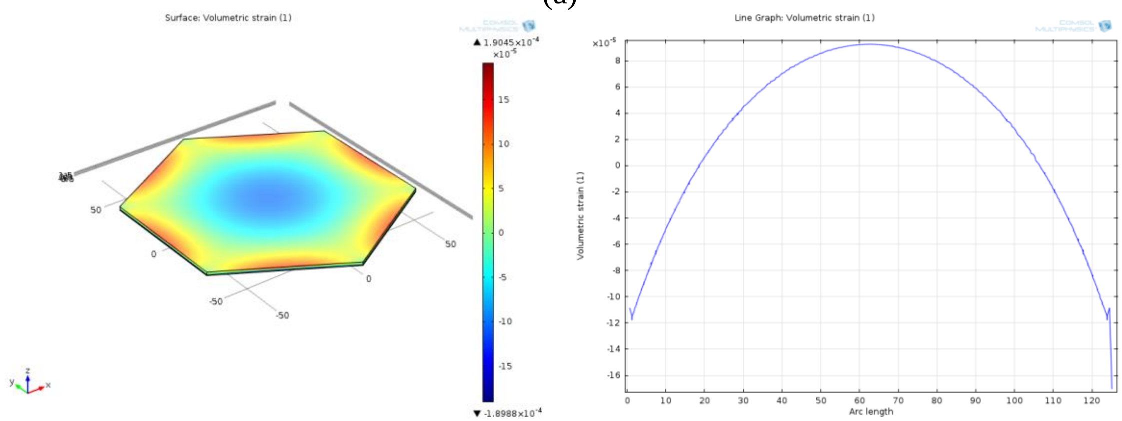

(b)

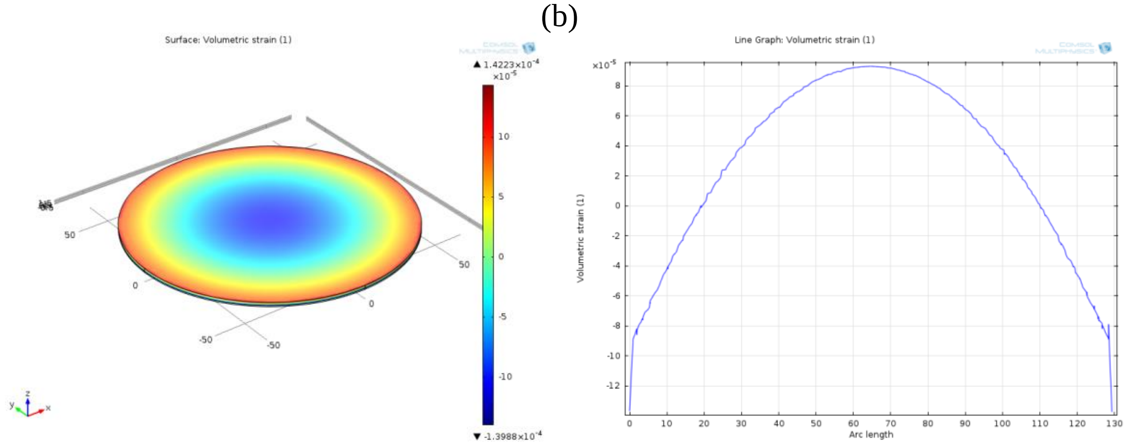

(c)

Figure 10. Simulated strain analysis of (a) square, (b) hexagon, and (c) circular CMUT membranes.

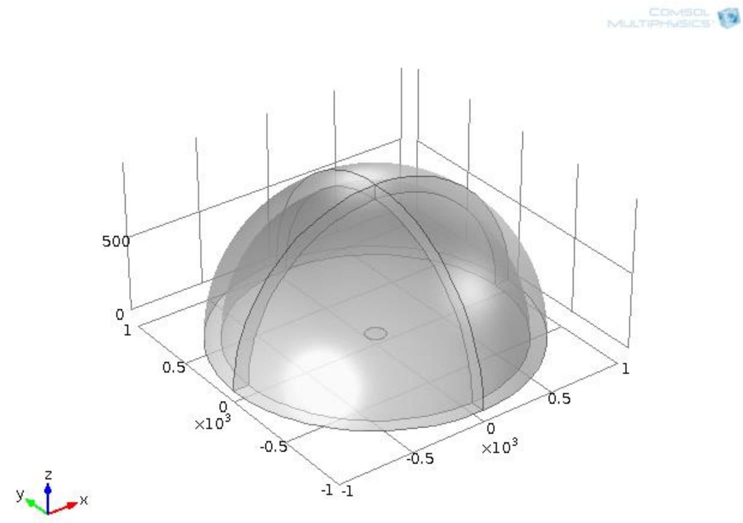

(a)

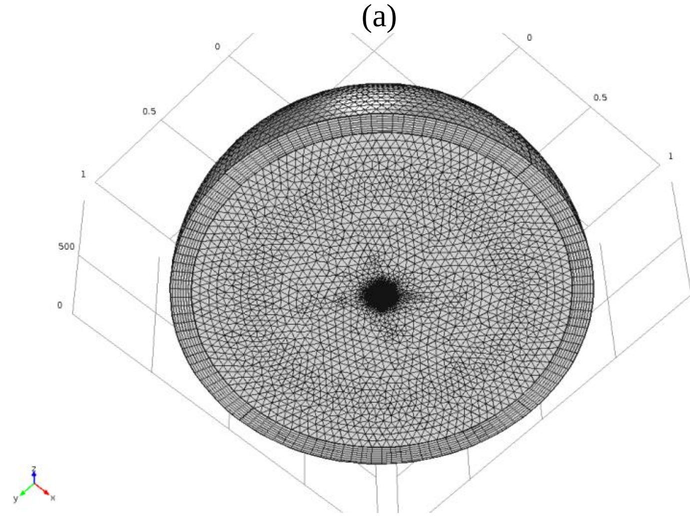

(b)

Figure 11. Simulated CMUT design for acoustic pressure output. (a) represents the simulated design for CMUT based on Table 2. (b) shows the meshing properties applied to each CMUT shape.

comparison to the other geometries which correlates with producing a greater acoustic pressure output. The rigidity of the square membrane limits its dynamic movement while vibrating therefore causing it to produce a smaller output.

In contrast, the Sound Pressure Level (SPL) generated by the three geometries were plotted in Fig. 13. The square has the highest maximum SPL at 128.55 dB, followed by hexagon at 128.39 dB, and lastly circular at 128.38 dB. Additionally, Table 6 compares the strength of SPL produced from each CMUT cell as a function of distance from the top of each cell membrane. Due to attenuation and the increase in distance from the top of the membrane, square and hexagon SPL strength reduces approximately 18 percent and circular reduces approximately 19 percent when measuring from 50 µm to 900 µm.

Table 6. Strength of SPL For Three Cell Geometries Versus Distance

Point Location (x, y, z)	Square SPL (dB)	Hexagon SPL (dB)	Circle SPL (dB)
(0,0,50 µm)	123.67	123.22	123.13
(0,0,100 µm)	119.55	118.94	118.81
(0,0,500 µm)	106.39	105.65	105.58
(0, 0, 900 µm)	101.19	100.46	100.22

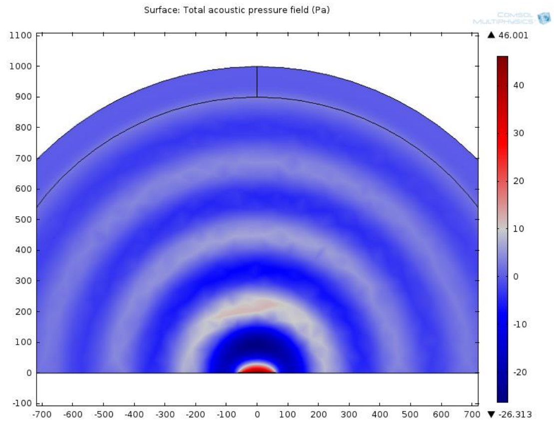

(a)

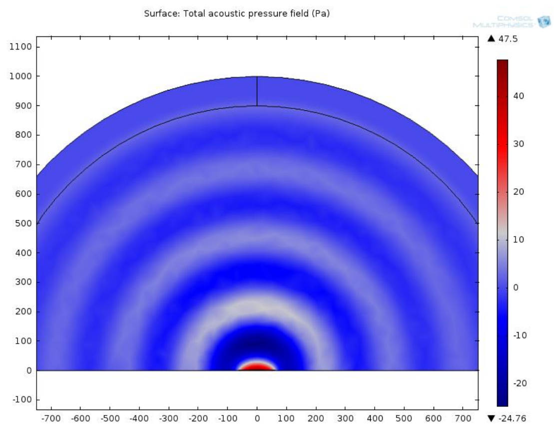

(b)

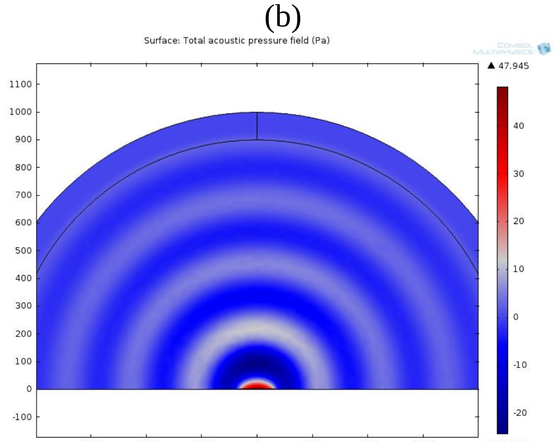

(c)

Figure. 12. Acoustic pressure output transmitting through air dome for a (a) square, (b) hexagon, and (c) circular CMUT cells operating at 1.5 MHz. The maximum acoustic pressure generated for the square, hexagon, and circular membranes are approximately 46.00 Pa, 47.50 Pa, and 47.95 Pa, respectively.

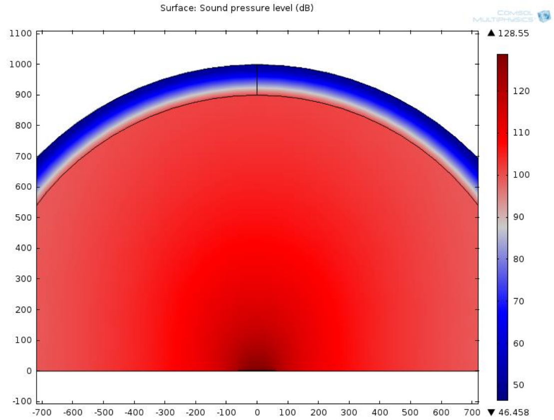

(a)

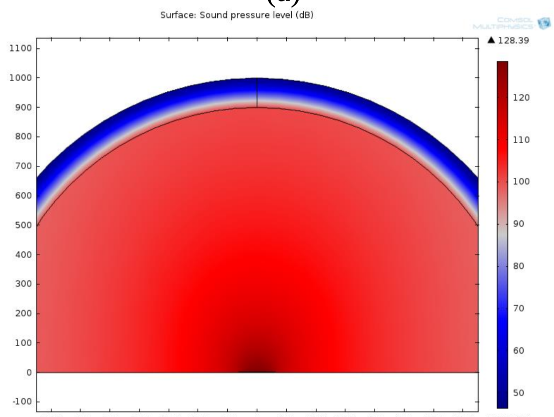

(b)

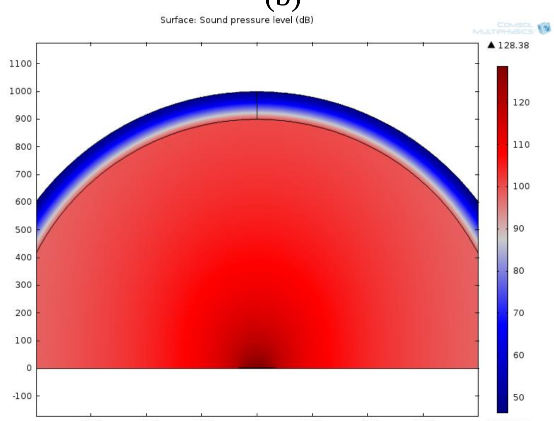

(c)

Figure 13. Sound Pressure Level (SPL) transmitting through air dome for (a) square, (b) hexagon, and (c) circular CMUT cells operating at 1.5 MHz. The maximum SPL generated for the square, hexagon, and circular membranes are approximately 128.55 dB, 128.39 dB, and 128.38 dB, respectively.

4. CONCLUSION

The emergence of Capacitive Micromachined Ultrasonic Transducers (CMUTs) to compete with piezoelectric micromachined ultrasonic transducers (PMUTs) is currently possible due to introducing advantages that overcome the weaknesses of this established technology. This technology evolution that integrates MEMS principles improves impedance matching, broadens immersion bandwidth, enables fabrication of on-chip integration, and increases acoustic wave transmission through fluid mediums. Operating as an oscillating system that transmits and/or receives ultrasonic waves, CMUT characteristics can be optimized to successfully be fabricated and implemented in various ultrasonic transducer applications.

In this research, three of the most tested membrane geometries were designed and simulated in COMSOL Multiphysics to compare influential parameters for CMUT technology such as resonance frequency, array density, electromechanics operation, spring stiffness, and acoustic pressure output. Based on the results, hexagon is in competition with circular membranes by having the highest packaging array density and produces similar acoustic pressure output values as the circular membrane. The flexibility of the circular shape compared to the other membrane shapes is an advantage. The higher flexibility of the membrane, due to a lower spring stiffness, reduces the amount of applied voltage necessary to operate the CMUT device. This indicates that less applied voltage is needed to generate maximize membrane deflection. A lower distribution of stress and strain for circular membranes in operation is also an advantage. Reducing the concentration of stress and strain on the device reduces the chance of fracturing or fatigue.

This research is a beneficial guideline on CMUT operation and introduces factors for CMUT design optimization that are ideal for devices operating at frequency ranges around 1.5 MHz. Various applications that operate within 1.5 MHz can include nondestructive imaging and ultrasonic medical equipment [31] as well as any air-coupling CMUT applications.

5. FUTURE WORK

In this thesis, three different CMUT cells were analytically analyzed and compared through simulation utilizing FEM. Rather than the main focus be on optimal CMUT cell design, we can select a single CMUT cell geometry and design fully operational devices while validating the acoustic pressure output generated by CMUT cells, study array distribution, study acoustic pressure output for multi-dimensional CMUT cells operating at the same frequency and improve on the directivity of transmitted acoustic waves. In this paper, the surrounding medium was air. The next step is to analyze how various surrounding mediums influence acoustic waves as well as how mediums influence membrane deflection. These mediums can include but are not limited to air at various temperatures, oil, and water. Additionally, factors that will possibly need to be considered include damping effects on CMUT operation and change in operating frequency [32, 33].

This research can also be extended by designing three fully functional square, hexagon, and circular CMUT devices, simulating each shape, and analyzing the influential parameters overtime. A time dependent study introduces measurable factors such as the change in acoustic pressure over time, the amount of time it takes for each CMUT cell to reach maximum acoustic pressure and monitoring the stress and strain distribution across the membrane over an extended period of time. The next step and ultimate goal for this research is begin the fabrication process. Utilizing the influential factors introduced, a CMUT device can be designed and fabricated so we can perform experimental tests and validate previous findings.

REFERENCES

[1] M. K. Mishra, V. Dubey, P. M. Mishra, and I. Khan, “MEMS Technology: A Review,” *J. Eng. Res. Rep.*, pp. 1–24, Feb. 2019, doi: 10.9734/jerr/2019/v4i116891.

[2] A. S. Algamili *et al.*, “A Review of Actuation and Sensing Mechanisms in MEMS-Based Sensor Devices,” *Nanoscale Res. Lett.*, vol. 16, no. 1, p. 16, Jan. 2021, doi: 10.1186/s11671-021-03481-7.

[3] J. Jung, W. Lee, W. Kang, E. Shin, J. Ryu, and H. Choi, “Review of piezoelectric micromachined ultrasonic transducers and their applications,” *J. Micromechanics Microengineering*, vol. 27, no. 11, p. 113001, Sep. 2017, doi: 10.1088/1361-6439/aa851b.

[4] A. S. Ergun, G. G. Yaralioglu, and B. T. Khuri-Yakub, “Capacitive micromachined ultrasonic transducers: Theory and technology,” *MEMS - Microelectromechanical Syst.*, vol. 16, no. 2, pp. 76–84, 2003, doi: 10.1061/(ASCE)0893-1321(2003)16:2(76).

[5] “What is MEMS Technology?,” *MEMs & Nanotechnology Exchange*. https://www.mems-exchange.org/MEMS/what-is.html (accessed May 01, 2021).

[6] M. Pappalardo, G. Caliano, A. S. Savoia, and A. Caronti, “Micromachined Ultrasonic Transducers,” in *Piezoelectric and Acoustic Materials for Transducer Applications*, A. Safari and E. K. Akdoğan, Eds. Boston, MA: Springer US, 2008, pp. 453–478. doi: 10.1007/978-0-387-76540-2_22.

[7] C. B. Doody, Xiaoyang Cheng, C. A. Rich, D. F. Lemmerhirt, and R. D. White, "Modeling and Characterization of CMOS-Fabricated Capacitive Micromachined Ultrasound Transducers," *J. Microelectromechanical Syst.*, vol. 20, no. 1, pp. 104–18, Feb. 2011, doi: 10.1109/JMEMS.2010.2093559.

[8] I. O. Wygant *et al.*, "50 kHz capacitive micromachined ultrasonic transducers for generation of highly directional sound with parametric arrays," *IEEE Trans. Ultrason. Ferroelectr. Freq. Control*, vol. 56, no. 1, pp. 193–203, 2009, doi: 10.1109/TUFFC.2009.1019.

[9] H. Wang, X. Wang, C. He, and C. Xue, "Design and Performance Analysis of Capacitive Micromachined Ultrasonic Transducer Linear Array," *Micromachines*, vol. 5, no. 3, Art. no. 3, Sep. 2014, doi: 10.3390/mi5030420.

[10] R. Sharma, R. Agarwal, A. K. Dubey, and A. Arora, "Pragmatics of capacitive micromachined ultrasonic transducer," in *2017 International Conference on Emerging Trends in Computing and Communication Technologies (ICETCCT)*, Nov. 2017, pp. 1–4. doi: 10.1109/ICETCCT.2017.8280328.

[11] W. Zhang, H. Zhang, Y. Wang, F. Du, S. Jin, and Z. Zeng, "Simulation characterization of CMUT with vented square membrane," in *2015 International Conference on Optical Instruments and Technology: Micro/Nano Photonics and Fabrication*, Aug. 2015, vol. 9624, p. 962406. doi: 10.1117/12.2192802.

[12] M. S. Salim, M. F. Abd Malek, R. B. W. Heng, K. M. Juni, and N. Sabri, "Capacitive Micromachined Ultrasonic Transducers: Technology and Application," *J. Med. Ultrasound*, vol. 20, no. 1, pp. 8–31, Mar. 2012, doi: 10.1016/j.jmu.2012.02.001.

[13] H. Wang *et al.*, “Hybrid Cell Structure for Wideband CMUT: Design Method and Characteristic Analysis,” *Micromachines*, vol. 12, no. 10, Art. no. 10, Oct. 2021, doi: 10.3390/mi12101180.

[14] R. Sharma, R. Agarwal, and A. Arora, “Evaluation of Ultrasonic Transducer with Divergent Membrane Materials and Geometries,” in *Smart Trends in Information Technology and Computer Communications*, Singapore, 2016, pp. 779–787. doi: 10.1007/978-981-10-3433-6_93.

[15] K. Brenner, A. S. Ergun, K. Firouzi, M. F. Rasmussen, Q. Stedman, and B. (Pierre) Khuri–Yakub, “Advances in Capacitive Micromachined Ultrasonic Transducers,” *Micromachines*, vol. 10, no. 2, Art. no. 2, Feb. 2019, doi: 10.3390/mi10020152.

[16] M. B. Thacker and D. A. Buchanan, “Design and Characterization of low frequency Capacitive Micromachined Ultrasonic Transducer (CMUT),” in *2020 IEEE International Conference on Systems, Man, and Cybernetics (SMC)*, Oct. 2020, pp. 2876–2881. doi: 10.1109/SMC42975.2020.9282903.

[17] P. Priya, B. D. Pant, B. Pilani, and C.-C. Pilani, “Capacitive Micro-machined Ultrasonic Transducer (CMUT) Based Volumetric Blood Flow-meter,” p. 7, 2015.

[18] R. Sharma, R. Agarwal, A. K. Dubey, and A. Arora, “Design and analysis of capacitive micromachined ultrasonic transducer,” *Recent Pat. Eng.*, vol. 13, no. 2, pp. 108–116, 2019, doi: 10.2174/1872212112666180214141506.

[19] Aditi, R. Mukhiya, K. Prabakar, M. Raghuramaiah, V. K. Khanna, and R. Gopal, “Experimental investigation on dynamic characteristics of hexagonal CMUT,” *Microsyst. Technol.*, vol. 25, no. 8, pp. 3053–3059, Aug. 2019, doi: 10.1007/s00542-019-04314-5.

[20] E. Ventsel and T. Krauthammer, *Thin Plates and Shells : Theory, Analysis, and Applications*, 1st ed. CRC Press, 2001. doi: 10.1201/9780203908723.

[21] I. O. Wygant, M. Kupnik, and B. T. Khuri-Yakub, "Analytically calculating membrane displacement and the equivalent circuit model of a circular CMUT cell," in *2008 IEEE International Ultrasonics Symposium, IUS 2008, November 2, 2008 - November 5, 2008*, Beijing, China, 2008, pp. 2111–2114. doi: 10.1109/ULTSYM.2008.0522.

[22] J. Mendoza-López and C. Sánchez-López, "Electromechanical performance comparison for different CMUT element geometries," in *2012 International Conference on Synthesis, Modeling, Analysis and Simulation Methods and Applications to Circuit Design (SMACD)*, Sep. 2012, pp. 109–112. doi: 10.1109/SMACD.2012.6339429.

[23] K. Bowman, "Mechanical Properties: Elastic Behavior," in *Encyclopedia of Condensed Matter Physics*, F. Bassani, G. L. Liedl, and P. Wyder, Eds. Oxford: Elsevier, 2005, pp. 286–291. doi: 10.1016/B0-12-369401-9/00568-4.

[24] M. Long, "2 - Fundamentals of Acoustics," in *Architectural Acoustics (Second Edition)*, 2nd ed., M. Long, Ed. Boston: Academic Press, 2014, pp. 39–79. doi: 10.1016/B978-0-12-398258-2.00002-7.

[25] H. Zhang, D. Liang, Z. Wang, L. Ye, X. Rui, and X. Zhang, "Fabrication and Characterization of a Wideband Low-Frequency CMUT Array for Air-Coupled Imaging," *IEEE Sens. J.*, vol. 20, no. 23, pp. 14090–14100, Dec. 2020, doi: 10.1109/JSEN.2020.3007068.

[26] Y. Huang, A. S. Ergun, E. Haeggstrom, M. H. Badi, and B. T. Khuri-Yakub, "Fabricating capacitive micromachined ultrasonic transducers with wafer-bonding technology," *J. Microelectromechanical Syst.*, vol. 12, no. 2, pp. 128–137, Apr. 2003, doi: 10.1109/JMEMS.2003.809968.

[27] A. S. Erguri, Y. Huang, X. Zhuang, O. Oralkan, G. G. Yarahoglu, and B. T. Khuri-Yakub, "Capacitive micromachined ultrasonic transducers: fabrication technology," *IEEE Trans. Ultrason. Ferroelectr. Freq. Control*, vol. 52, no. 12, pp. 2242–2258, Dec. 2005, doi: 10.1109/TUFFC.2005.1563267.

[28] "COMSOL Multiphysics User Guide," 2020. https://doc.comsol.com/5.6/docserver/#!/com.comsol.help.comsol/helpdesk/helpdesk.html

[29] A. I. Shaikh and N. N. Deshmukh, "Theoretical, Simulation and Experimental Analysis of Sound Frequency and Sound Pressure Level of Different Air Horn Amplifier," *Int. J. Eng. Res. Technol.*, vol. 4, no. 2, Mar. 2015, Accessed: Mar. 31, 2022.

[30] A. İ. Yaşar, F. Yıldız, and O. Eroğul, "Capacitive micromachined ultrasonic transducer: transmission performance evaluation under different driving parameters and membrane stress for underwater imaging applications," *Microsyst. Technol.*, vol. 26, no. 12, pp. 3601–3611, Dec. 2020, doi: 10.1007/s00542-020-04827-4.

[31] J. Joseph, B. Ma, and B. T. Khuri-Yakub, "Applications of Capacitive Micromachined Ultrasonic Transducers: A Comprehensive Review," *IEEE Trans. Ultrason. Ferroelectr. Freq. Control*, pp. 1–1, 2021, doi: 10.1109/TUFFC.2021.3112917.

[32] B.-S. Cha, T. Kanashima, S.-M. Lee, and M. Okuyama, “Air damping effect on the air-based CMUT operation,” *J. Korean Phys. Soc.*, vol. 67, pp. 486–495, Aug. 2015, doi: 10.3938/jkps.67.486.

[33] M. R. Stoker, “Principles of pressure transducers, resonance, damping and frequency response,” *Anaesth. Intensive Care Med.*, vol. 5, no. 11, pp. 371–375, Nov. 2004, doi: 10.1383/anes.5.11.371.53397.